https://dx.doi.org/10.1016/j.ijmecsci.2021.106328



# A simplified analytical model for the investigation of contact acoustic nonlinearity in pipe structures

Ruiqi Guan[1], Ye Lu[2]*, Fangxin Zou[1], Kai Wang[3], Zhongqing Su[3]

[1]Interdisciplinary Division of Aeronautical and Aviation Engineering, The Hong Kong Polytechnic University, Hung Hom, Kowloon, Hong Kong SAR, China

[2]Department of Civil Engineering, Monash University, Clayton, VIC, Australia

[3]Department of Mechanical Engineering, The Hong Kong Polytechnic University, Hung Hom, Kowloon, Hong Kong SAR, China

## Abstract

A simplified analytical model of contact acoustic nonlinearity (CAN) in pipe structures was established and verified by finite element modelling to analyse the multimode second harmonic waves induced by a breathing crack. The analytical model was developed from plate to pipe structures with S-parameter formulation applied for the investigation of second harmonic generation where pure longitudinal wave mode excitation was used. A numerical simulation model with the same excitation condition was developed to confirm the results from the theoretical analysis. Multimode second harmonic waves were obtained in both analytical and simulation models and the proportion of different modes in terms of axial amplitude was also studied. A new nonlinear index was finally proposed for the quantitative assessment of fatigue crack growth in pipe structures.

**Keywords:** Contact acoustic nonlinearity, pipe structures, analytical model, multimodal second harmonic waves.

## 1. Introduction

Guided wave-based damage detection with linear characteristics has been widely applied in pipe structures. Given the increasing demand for the damage detection at early stages, nonlinear guided waves with high sensitivity to microscale damage have drawn the attention of many researchers. Techniques using nonlinear ultrasonic guided waves have shown great capability for damage identification in structures using nonlinear ultrasonic behaviour including higher-harmonic generation [1-6], mixed frequency response [7-12] and sub-harmonic generation [13-15]. Nonlinear ultrasonics can be grouped into four types: classical nonlinear elasticity, contact acoustic nonlinearity (CAN), hysteresis and non-classical dissipation [16]. It should be noted that the mechanisms of nonlinearity are complex; sometimes similar nonlinear effects can be manifested by different physical mechanisms, and vice versa [16]. Among these mechanisms, classical nonlinear elasticity and CAN exist commonly and usually simultaneously in engineering structures with microscale damage such as initial fatigue cracks and corrosion pits.

Material nonlinearity has been widely studied theoretically and experimentally. It may exist homogeneously in the structure material or appear as localised damage around the crack tip with plastic deformation [17-20]. At location of stress concentration, such as holes and/or notches in the structure, a single microcrack mostly initiates at the edge of

these features and gradually grows to a larger size under fatigue load. In this case, CAN occurs when ultrasonic waves pass through the interface between two surfaces of the microcrack. As the incident wave approaches a contact interface, the compressional and tensile parts cause closing and opening of the crack, which induces localised nonlinearity.

In the past few years, different analytical models of CAN in plate structures have been developed. The first model of such nonlinearity was provided by Richardson [21]. This model contains two semi-infinite elastic materials with intimate contact separated by a planar interface, across which no traction forces exist. Another model considered the contact between two rough surfaces with changeable contact area under applied stress, which induced nonlinearity of the interface [22]. This model acts as a nonlinear spring with varying stiffness when stress is applied. A more popular model for CAN was called the bi-linear stiffness model [23]. It had different stiffnesses under compression and tensile phases of a wave and the crack became similar to a “mechanical diode”. This local stiffness effect was also studied when using shear wave mixing at crack interface [24]. Theoretical crack model considering roughness, friction and hysteresis was proposed [25], which brought insight into the model with more complex conditions. Further development of the CAN model introduced the generation of crack-induced second source stress (CISS), which treated the breathing crack as a second source of generation of stress waves, promoting the analytical model into 3D scenario [26]. The total force of the second source was calculated as an integration of the stress on the crack surface and was modified by a function related to the durations of crack opening

and closing. Then the received amplitude of waves at double frequency could be derived based on elastodynamic analysis. This method provided a nonlinear index for quantitative assessment of CAN in a plate structure.

Although theoretical analysis of CAN in plate structures was undertaken by many researchers, theoretical analysis of nonlinear guided waves in pipe structures was quite limited, with most focusing on material nonlinearity [27-29]. Guided wave propagations in pipe structures are more complex and multiple wave modes are induced by damage attributable to the structural curvature[30, 31]. Therefore, analysis of the generation of second harmonic waves in a pipe structure and a proper nonlinear index are both in high demand for the measurement of CAN.

Apart from the analytical model analysis of CAN, different numerical methods were also developed to study the interaction between guided waves and close crack in a structure, including finite discrete element method (FDEM) [32], local interaction simulation approach (LISA) [33-35], finite difference time domain method (FDTD) [36, 37], time-domain spectral finite method [38] and finite element method (FEM) [39, 40]. The FEM model was adopted widely for the development of CAN model in both steel and composite components [41, 42]. Meanwhile, various crack interface in FEM model was established and studied for CAN, including seam crack [40, 43-45] and crack with rough contact or friction [46-50].

In this study, the 3D analytical method with CISS adopted in the plate was referred for the establishment of an analytical model in a pipe structure. A simplified analytical

model based on S-parameter formulation was developed to analyse the second harmonic generation in a pipe. Pure longitudinal wave mode in the pipe was excited and the amplitudes of multiple wave modes induced by the breathing crack at second harmonic were calculated and after which the proportion of each second harmonic wave mode in terms of axial amplitude was evaluated. Validation of the analytical model was implemented using FEM and a new nonlinear index for measurement of the severity of CAN in a pipe structure was proposed.

## 2. Methods

Due to the curvature of pipe structures, theoretical analysis in a 3D pipe was usually semi-analytical combined with numerical simulation. In this study, a simplified condition was assumed where only longitudinal wave mode was excited and the theory of scattering of waves in an elastic hollow cylinder with S-parameter in the linear method was used to derive the second harmonic waves induced by the breathing crack.

When the guided wave propagates in a pipe structure with a microcrack in the middle of it as in Figure 1, the wave interacts with the crack and multiple wave modes subsequently generate. The general expansion of generated wave displacement field by the circumferential crack at location $z_c$ is similar with the case where linear guided waves are scattered by a crack [51]

$$\begin{cases} \boldsymbol{u}_{\boldsymbol{\mu}}^{\boldsymbol{N}}(r,\theta,z) = \sum_{\mu,N} C_{\boldsymbol{\mu}+}^{\boldsymbol{N}}(z)\boldsymbol{u}_{\boldsymbol{\mu}+}^{\boldsymbol{N}}(r,\theta) & z > z_c \\ \boldsymbol{u}_{\boldsymbol{\mu}}^{\boldsymbol{N}}(r,\theta,z) = \sum_{\mu,N} C_{\boldsymbol{\mu}-}^{\boldsymbol{N}}(z)\boldsymbol{u}_{\boldsymbol{\mu}-}^{\boldsymbol{N}}(r,\theta) & z < z_c \end{cases}, \quad (1)$$

where $\mu$ and N denote the group order and the circumferential order of a mode, respectively; $C_{\mu+}^{N}(z)$ and $C_{\mu-}^{N}(z)$ represent the amplitude of generated waves when $z > z_c$ and $z < z_c$, respectively; $\boldsymbol{u}_{\boldsymbol{\mu+}}^{\boldsymbol{N}}(r,\theta)$ and $\boldsymbol{u}_{\boldsymbol{\mu-}}^{\boldsymbol{N}}(r,\theta)$ are the model particle displacement in the region $z > z_c$ and $z < z_c$ respectively and

$$\boldsymbol{u}_{\mu\pm}^{N}(r,\theta) = \sum_{\alpha=r,\theta,z} \boldsymbol{R}_{\mu\alpha}^{N}(r)\boldsymbol{\Theta}_{\alpha}^{N}(N\theta), \tag{2}$$

where the functions $\boldsymbol{R}_{\mu\alpha}^{N}(r)$ and $\boldsymbol{\Theta}_{\alpha}^{N}(N\theta)$ are the radial and angular characteristic functions; $\boldsymbol{R}$ is related to Bessel functions and modified Bessel functions and was calculated through reference [52]; $\boldsymbol{\Theta}$ contains sines and cosines of N$\theta$.

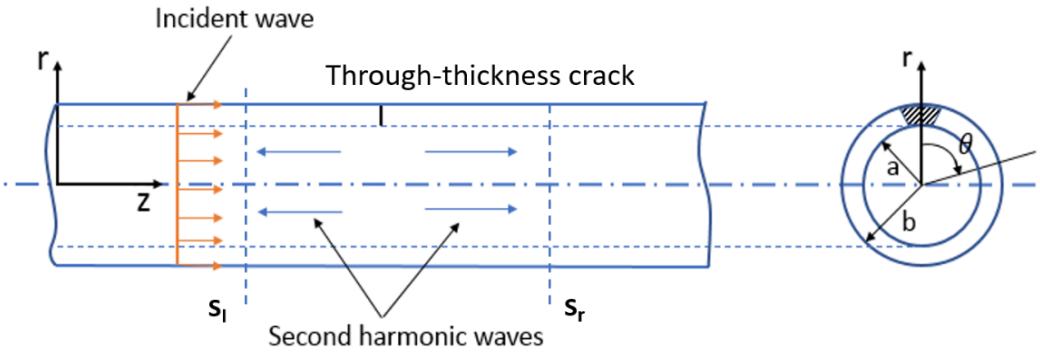


Figure 1 Configuration of analytical pipe model with longitudinal wave excitation and breathing crack as a second wave source in the pipe. The crack is through thickness and the extent of crack is along $\theta$ axis.

The relation between amplitudes $C_{\mu\pm}^{N}(z)$ and S-parameter can be expressed as

$$C_{\mu\pm}^{N}(z = z_{\lambda,\kappa}) = \sum_{\nu,\kappa,M} S_{\mu\lambda;\nu\kappa}^{N,M} a_{\nu\kappa}^{M}, \tag{3}$$

where $\lambda$ and $\kappa$ denote left or right reference plane in the pipe; $\nu$ and $M$ denote the group order and the circumferential number of the incident mode; $a_{\nu\kappa}^{M}$ are the amplitudes of the incident wave mode on either plane of the pipe. When the wave propagates in the pipe and interacts with the closed crack, the crack is treated as a second source which induces stress in the pipe and the passing waves are modulated by the breathing behaviour of the crack. Therefore, stress induced by the breathing crack in the pipe needs to be investigated, and the S-parameter needs to be modified based on a pure longitudinal excitation and a breathing crack as the second source.

# 3. Analytical model establishment and numerical method validation of interaction between guided waves and closed crack

## *3.1 Analytical model*

As shown in Figure 1, pure longitudinal wave was excited in this analytical study and the location of the closed microcrack was $z_c$ along the z axis. Reference planes at left and right were labelled for the S-parameter formulation.

As in reference [26], the modulated stress on the breathing crack surface was treated as a second source which generated second harmonic waves. In this study, it is assumed that the incident longitudinal wave stress which caused a displacement at the crack was simply equivalent to the stress on the crack surface. Since the microscale crack is sufficiently small when it was compared with the distance between the excitation and the monitoring points, the total stress on the crack surface when it is open was

equivalent to a point load and calculated as the integration of the stress over the crack surface.

$$F_{open} = \int_S \boldsymbol{T}_{inc}(zz)\, dS, \tag{4}$$

where $\boldsymbol{T}_{inc}(zz)$ is the axial component stress tensor of incident wave; *S* denotes the crack surface area.

The point load would be modified during the crack's opening and closing behaviour. Meanwhile, the breathing behaviour caused diffraction at the tip of the crack, which was circumferential shear horizontal (SH) wave propagating in the circumferential direction, and it disturbed the duration of crack opening and closing. The duration of diffraction was estimated as the time of wave travelling from the middle of the crack to the tip, which is $\frac{LT_{inc}}{2\lambda_{SH}}$, while the duration of crack opening due to the stress on the crack is $\frac{T_{inc}}{2}$. $\lambda_{SH}$ is the wavelength of the circumferential SH wave and L is the crack length. With the duration of crack closing and opening, the stress field on the crack was modulated by a function [53]

$$f(t) = \begin{cases} 1, & t_{open} < t < t_{close} \\ 0, & t_{close} < t < t_{open} + \frac{T_{inc}}{2} + \frac{LT_{inc}}{2\lambda_{SH}} \end{cases}, \tag{5}$$

at the angular frequency $\omega_1$ of the excitation as

$$F_{crack,f_1} = F_{open} \cdot f(t) e^{iw_1 t}. \tag{6}$$

The relation between displacement of the crack node and the wave modulation function is plotted in Figure 2.

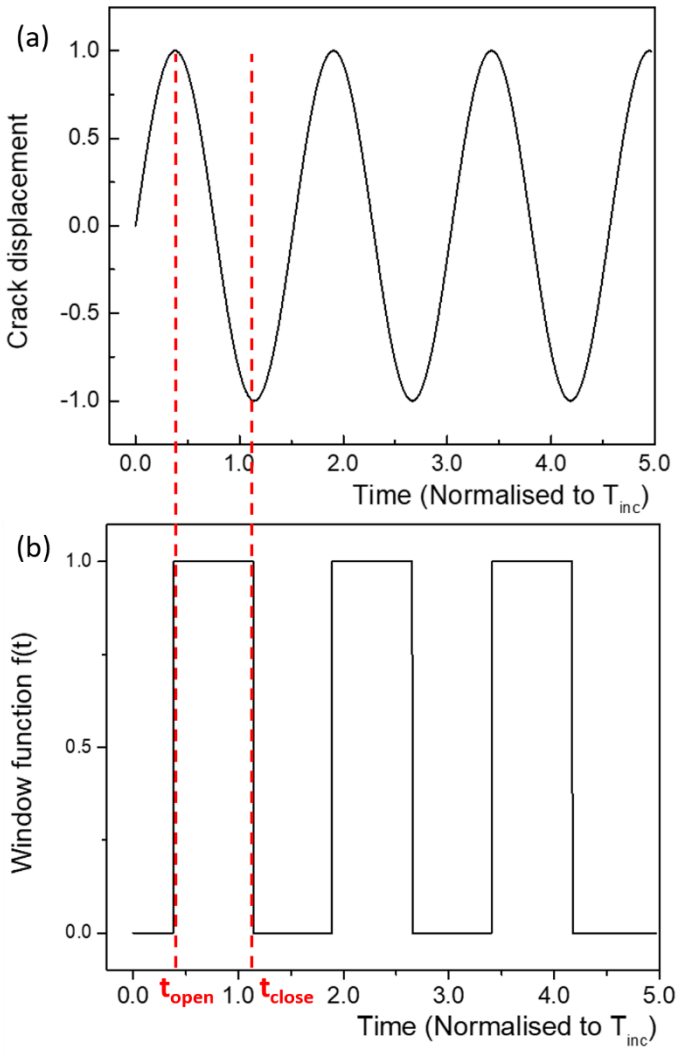


Figure 2 (a) Crack displacement under the incident wave. The red dash lines indicate the time of crack open $t_{open}$ and crack closed $t_{close}$. The period of crack displacement was influenced by the scattered circumferential SH waves. (b) Window function for the modulation of crack displacement field.

With the modulation function and the frequency spectrum of the crack surface displacement, the amplitude $A_{2f_1}$ at double frequency in the frequency spectrum can be obtained through Figure 3.

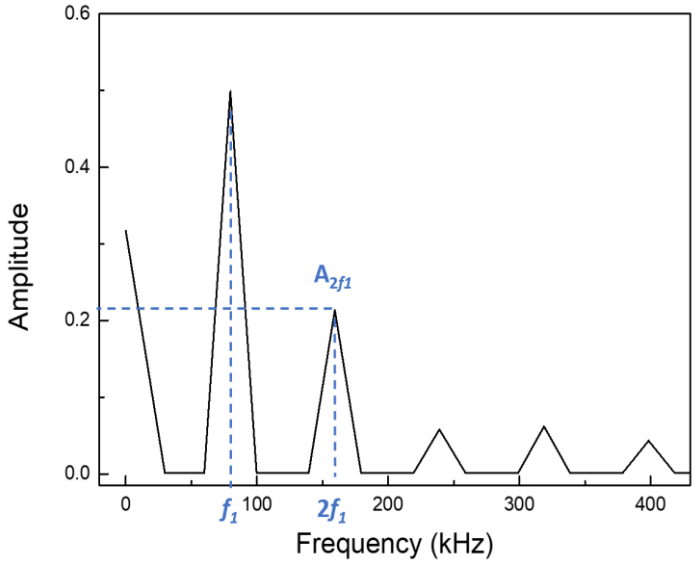


Figure 3 Frequency spectrum of displacement amplitude. Blue dash lines show the amplitudes at fundamental frequency $f_1$ and at double frequency $2f_1$.

As a result, the stress field on the crack at double frequency was modulated as

$$F_{crack,2f_1} = A_{2f_1} F_{open,f_1} \cdot e^{i2\omega_1 t} = e^{i2\omega_1 t} \int_S \boldsymbol{T}_{2f_1}(zz)\, dS, \qquad (7)$$

which can be treated as a second source with stress $T_{2f_1}$ to generate second harmonic waves at double frequency.

To further obtain the displacement field of generated second harmonic wave in the pipe, the S-parameter formulation was modified and deployed. When considering the incidence of longitudinal axisymmetric modes which satisfies the requirements that the mode has a large wavelength and an entirely axial stress field, and the crack was sufficiently long and through-thickness with angular extent α under uniform tension,

the general scattering formula for the guided waves by a crack in cylinders was approximated by elastostatic solutions [51]. As well, the S-parameter under longitudinal mode excitation can be simplified as [54, 55]

$$\tilde{S}^{\bar{N},0}_{\bar{\mu}l;\bar{\nu}l} = \frac{-i\omega_{zz}T^{0}_{\bar{\nu}}\bar{R}}{\sqrt{2}E\epsilon}\left\{\frac{\alpha\cos(\bar{N}\alpha)}{\bar{N}^{2}} - \frac{\sin(\bar{N}\alpha)}{\bar{N}^{3}}\right\}\int_{a}^{b} rR_{\bar{\mu}zz}(r)\,dr, \quad (8)$$

where $\tilde{S}^{\bar{N},0}_{\bar{\mu}l;\bar{\nu}l}$ stands for the S-parameter when the incident mode is a longitudinal wave and the circumferential order M=0, $\bar{R} = (a+b)/2$; $T^{0}_{\bar{\nu}}$ represents the magnitude of stress on the crack after modulation and $T^{0}_{\bar{\nu}} = T_{2f}$; $\alpha$ is half of the crack angle; E denotes the Young's modulus; $\epsilon^{2} = \frac{1}{[12(1-\nu^{2})]^{\frac{1}{2}}}(\frac{H}{\bar{R}})$; $\nu$ is the Poisson's ratio; $H = b - a$; $R_{\bar{\mu}zz}(r)$ consists of a modified Bessel function, which was calculated by equations in [56]; r is the coordinate along the radius direction. From Equation 8, it can be seen that the S-parameter changes with the extent of the angle of the crack and the trends are different for different wave modes. With the updated S-parameter, the axial displacements of second harmonic waves can be calculated by substituting Equations 2 and 3 into Equation 1.

It should be mentioned that material nonlinearity introduced by material dislocation around the tip of fatigue crack was not involved in the analytical model and only nonlinearity caused by the breathing behaviour of the microcrack was considered, since this study focuses on the mechanism of second harmonic generation related to CAN.

The study of this model was carried out based on an 80 mm outer diameter, 4 mm wall thickness aluminium pipe. To determine a proper excitation frequency for the generation of CAN and predict the second harmonic wave modes, the dispersion curves

of this pipe were plotted by DISPERSE® shown in Figure 4. It should be noticed that the notation from Rose [56] was adopted in the subsequent study, in which L(n, m) was defined as a longitudinal mode group, including axisymmetric modes L(0, m) and non-axisymmetric modes F(n, m). The integer *n* is the circumferential order of a mode and the integer *m* denotes the group order of a mode.

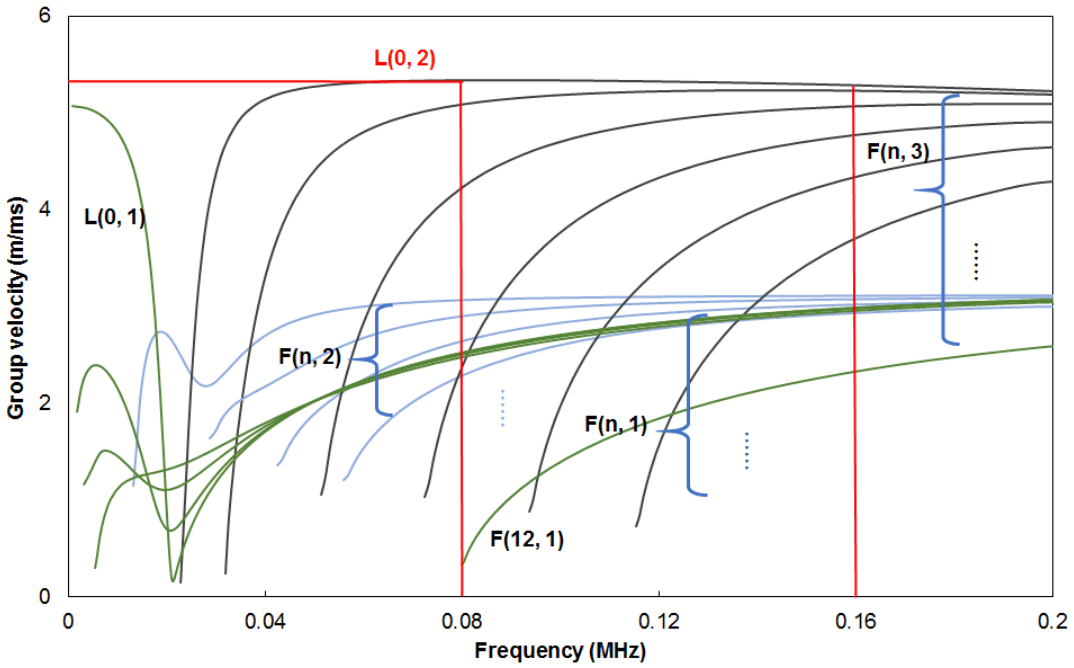

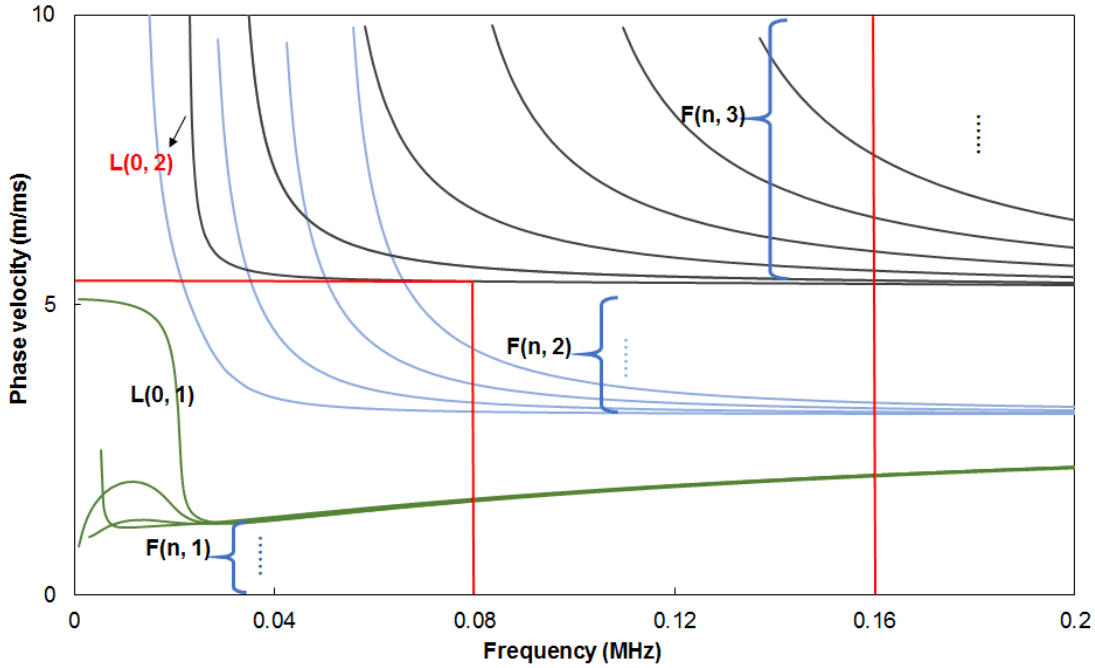


Figure 4 Dispersion curve of 80 mm outer diameter, 4 mm wall thickness aluminium pipe in terms of (a) group velocity and (b) phase velocity. Red lines indicate the excitation wave mode and frequency, and possible second harmonic waves generated at double frequency after interacting with the breathing crack.

The fundamental wave as the excitation was selected at 80 kHz and the wave mode is L(0, 2), the fastest wave mode around this frequency, which is also non-dispersive over a wide range of frequencies. It should be mentioned that the second harmonic waves should have infinite wave modes if the flexural wave modes were induced by the crack. In this study, the first five modes of flexural waves were studied since they cover the main portion of the nonlinearity.

### *3.2 Numerical analysis*

To validate the theoretical analysis results, finite element (FE) simulation was applied to model the interaction between a longitudinal wave and a closed crack in the pipe and all second harmonic wave modes were extracted from the simulation. A 3D FE model in Abaqus/Explicit was utilised to simulate the nonlinearity caused by the breathing crack. The pipe model had the same dimension as in the analytical model. The excitation signal was a 5-cycle Hanning-windowed tone burst signal at a central frequency 80 kHz. To achieve the convergence and accuracy of the computation, the minimum element length and time increment were selected as 1 mm and $5 \times 10^{-8}$ s respectively. The material properties of the aluminium are listed in Table 1.

Table 1 Material properties of 5 mm aluminium pipe.

| **Material properties** | **Density ($\rho$) (kg/m$^3$)** | **Young's Modulus (E) (GPa)** | **Poisson's Ratio ($\nu$)** |
|---|---|---|---|
| | 2700 | 70 | 0.33 |

To generate a pure longitudinal wave, the number of elements in the actuator ring should be greater than n, where n is the highest circumferential order of the flexural mode which has a cut-off frequency within the bandwidth of the excitation [57]. From the dispersion curve in terms of group velocity in Figure 4, the highest order flexural mode within the bandwidth of the excited L(0, 2) is F(12, 1). Therefore, for more accurate excitation, 16 elements should be assigned in the sensor ring. In this study, 16 actuator elements with 22.5-degree equivalent spacing were adopted and the excitation signal was applied as a point load at the node of the centre of each element along the

direction of the pipe axis. The transducer ring is 300 mm from the crack. The configuration of this model and the generated longitudinal wave in the pipe are shown in Figure 5. To enhance the second harmonic waves and remove the disturbance from the fundamental wave, after all excitation signals were received, a 180° out-of-phase inverse signal with the same waveform was excited in the pipe at the same location and was received following the same procedure. The combination of these two received signals would produce signals that contain nonlinearity at higher harmonics only.

To introduce a breathing crack in the pipe, a seam crack definition was used on each surface of the crack, which enabled breathing behaviour when waves interacted with the crack. Meanwhile, a surface-to-surface contact interaction and associated properties were defined on the crack interface to achieve the modelling of CAN. The crack was through the wall thickness and located in the middle of the pipe. The crack length in the circumferential direction was changed from 1 mm to 14 mm (0.01 to 0.21 after normalised by the wavelength of L(0, 2) mode at the fundamental frequency) with increments of 1 mm, and then from 14 m to 34 mm (0.21 to 0.50 after normalised by the wavelength of L(0, 2) mode at the fundamental frequency) with increments of 4 mm. Figure 5(a) and (b) show the process of ultrasonic guided waves interacting with the breathing crack. It can be seen that the stress induced by a wave transmits through the crack when it is closed but cannot pass through when the crack is open.

It should be mentioned that, material nonlinearity which is induced by the material plasticity at the early stage of the fatigue crack was not considered in the numerical model either, since this type of nonlinearity is marginal compared with CAN [26, 31] and

contributes less to the total nonlinearity as the crack propagates. The modelling in this study concerned about the microcrack initiation and growth in the pipe structures. Therefore, only the mechanism of CAN was considered when simulating the model.

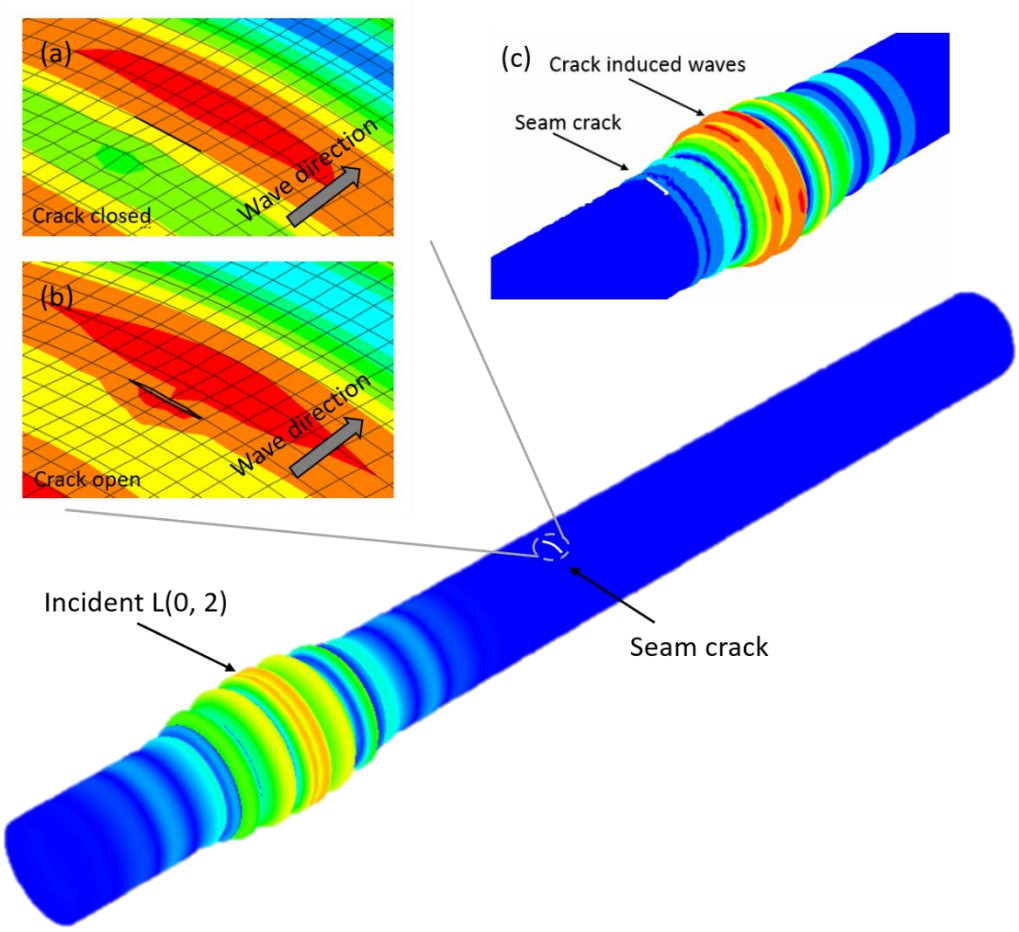


Figure 5 Configuration and displacement field of pipe model in simulation. Pure longitudinal L(0, 2) is excited in the model. (a) Crack is closed when the compressional part of the wave passes through. (b) Crack is open when the tensile part of the wave passes through. (c) Crack-induced second harmonic waves with non-axially symmetric displacements.

From the dispersion curve of this pipe, the second harmonic waves would be multiple wave modes including L(0, 2) and F(n, 3) at double frequency. Likewise, in the simulation model, more than one wave mode was generated after the incident wave

interacted with the crack, which can be observed by the non-axially symmetric displacement in Figure 5(c), indicating the existence of flexural waves after interaction with the crack. Thus, it is necessary to extract each mode so that they can be analysed separately. 16 monitoring points with the same spacing at 350 mm from the crack were assigned in the circumferential direction. All the points would receive signals at the same time in terms of the axial displacement, after which an appropriate signal separating method was applied on these received signals to obtain different modes at double frequency [58]. In detail, for the longitudinal mode, all signals from monitoring points were processed with a band pass filter in MATLAB at double frequency 160 kHz with a bandwidth of $\pm$ 15 kHz and the results are totalled to obtain the final signal. For the flexural modes, the same band pass filter was used on each of the received signals and then a phase delay of $N\theta/2\pi$ was applied to each signal, where N is the circumferential order and $\theta$ is the angular distance from the centre of the notch. Finally, the sum of these delayed signals would generate the corresponding flexural modes.

## 4. Results

### *4.1 Results from analytical model*

From the dispersion curve, it can be seen that at the double frequency, multiple wave modes exist. The axial displacements at the pipe surface of all second harmonic waves induced by the breathing crack were calculated with Equation 1 and the results are plotted with various crack lengths which are normalised by the wavelength of excited L(0, 2) mode at fundamental frequency, as shown in Figure 6.

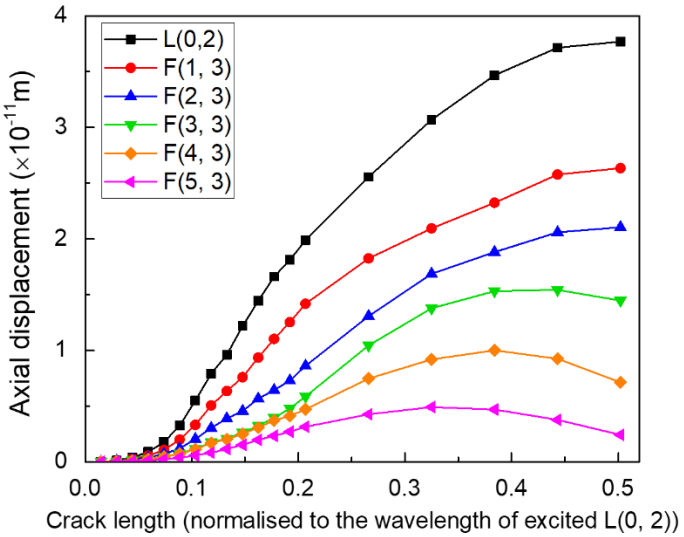


Figure 6 Displacement amplitudes of second harmonic waves including L(0, 2) and F(n, 3) (n=1,2,..5) derived from the analytical model with various crack lengths.

It is noticed that the trend of the first three modes L(0, 2), F(1, 3) and F(2, 3) keeps increasing monotonously, but for F(3, 3), F(4, 3) and F(5, 3), they start to decrease at around 0.5, 0.44 and 0.38 crack length. Therefore, within the crack length of 0.5, the first three modes are more suitable than higher order modes for the quantitative evaluation of crack length. This is similar to analysis with linear methods for pipe structures, where the guided wave is scattered by a circumferential crack and more than one wave mode is scattered. In those waves, the axisymmetric mode (n=0) was most efficiently scattered by the crack but the other modes did not change monotonically with the crack length [51]. Since multiple wave modes were generated as second harmonic waves, the proportion of different modes was calculated to investigate the contribution of each mode for the CAN. The percentage of each mode was calculated

as its respective axial displacement amplitude divided by the sum of amplitudes of all six modes, as shown in Figure 7 in terms of crack length.

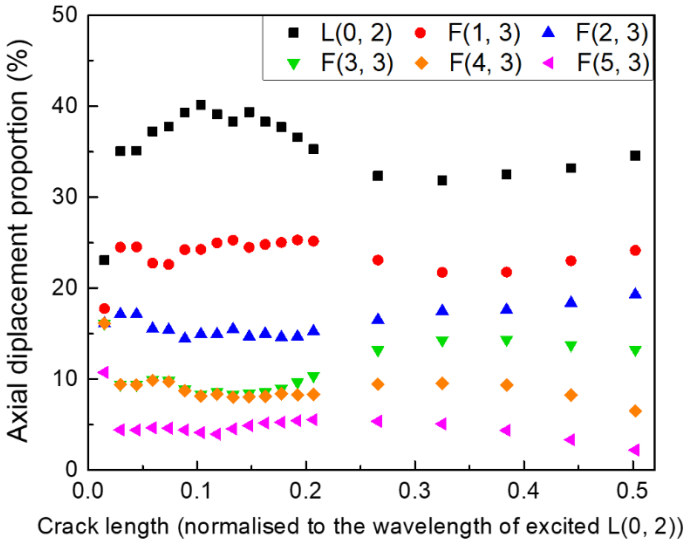


Figure 7 Proportion of different wave modes including L(0, 2) and F(n, 3) (n=1,2,..5) as second harmonic wave.

From Figure 7, it is obvious that L(0, 2) occupies the largest proportion of the total energy, and the percentage is higher when the crack length is less than 0.2. However, flexural modes at lower orders (n=1, 2) also take 15% to 25% of the total energy, which cannot be ignored when measuring the nonlinearity caused by the breathing crack. Furthermore, as the crack length increases, the proportion of flexural modes F(3, 3) increases, which may also be considered for nonlinearity evaluation.

The results from analytical study show that multiple wave modes would be generated after a longitudinal wave interacts with a breathing crack and the flexural waves play vital roles that must be considered when measuring the second harmonics caused by

CAN. It should be noticed that to use Equation 8 with elastostatic solutions, the length of the crack should satisfy $\alpha \sim O(\epsilon^2)$. For the pipe used here with $\upsilon$=0.33 and the thickness to mean radius ratio of 0.1, after the calculation of $\epsilon$ through the equation $\epsilon^2 = \frac{1}{[12(1-\nu^2)]^{\frac{1}{2}}}\left(\frac{H}{\bar{R}}\right)$, the minimum crack length is about 2.4 mm. It can be seen that in Figure 7, the first point for all wave modes has an obvious error because the crack length is only 1 mm at that point and the equation cannot perform well for this case.

### *4.2 Results from numerical analysis*

Some typical signals received from the simulation model with a 4 mm seam crack after signal processing at double frequency are shown in Figure 8, labelled L(0, 2), F(1, 3), F(2, 3) and F(3, 3). It is evident from the figures that the flexural waves arrive at almost the same time as L(0, 2), consistent with the dispersion curve, showing that the group velocity of the flexural wave modes is close to that of the longitudinal wave. The separation of flexural modes from the longitudinal mode is not ideally accurate for higher order modes which are highly dispersive, and may also be influenced by another group of flexural modes F(n, 2) as shown in the dispersion curve (Figure 4).

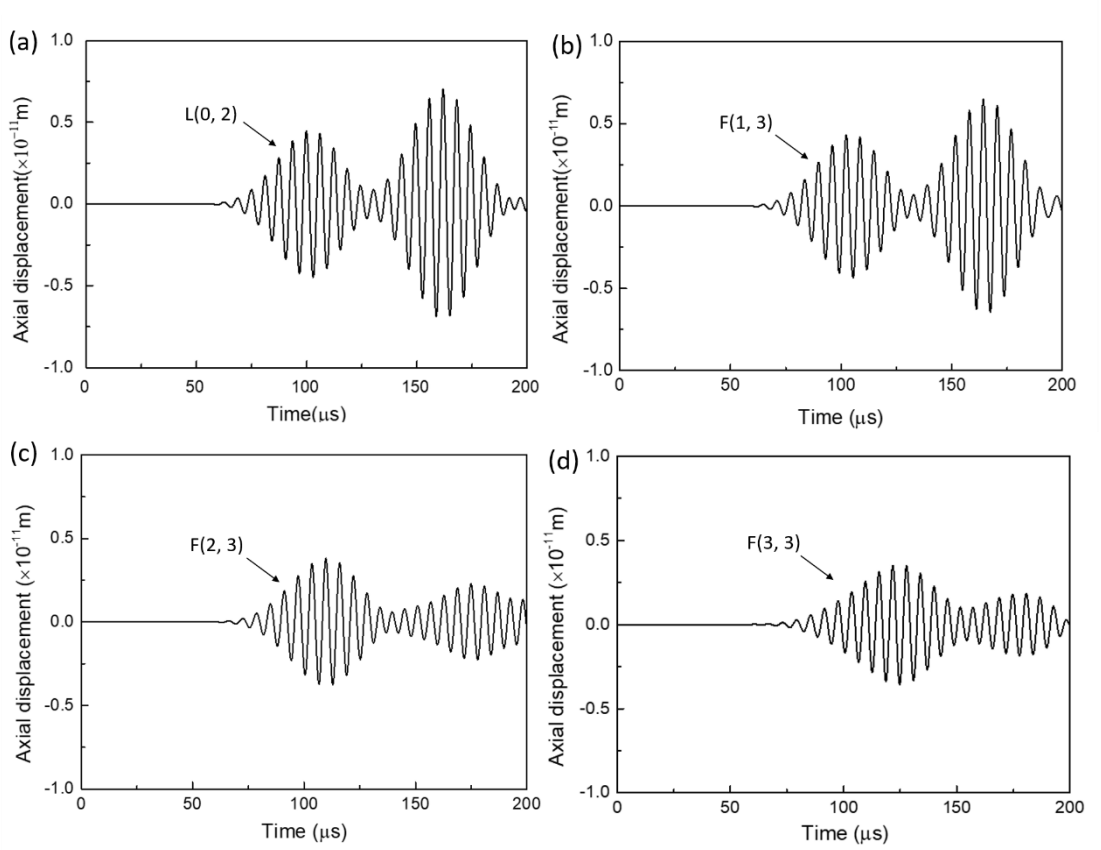


Figure 8 Signals at double frequency from simulation model with 4 mm seam crack of a) L(0, 2), b) F(1, 3), c) F(2, 3) and d) F(3, 3) modes.

To observe the changes in displacement amplitude of different second harmonic modes generated by different crack lengths, the axial displacement amplitude of each mode is also plotted with various crack lengths and is shown in Figure 9.

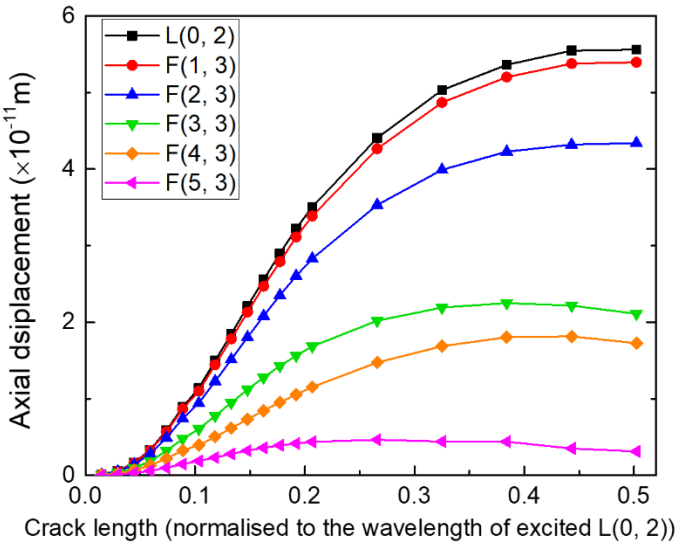


Figure 9 Axial displacement of different wave modes at double frequency with various crack lengths from simulation results.

Similar to the analytical results, the increasing trends of the first three modes are monotonous with the increase in crack length, while F(3, 3), F(4, 3) and F(5, 3) begin to decrease when the normalised crack lengths are 0.44, 0.5 and 0.32, respectively. The displacement amplitude of the flexural wave mode F(1, 3) is close to L(0, 2), which is different from the analytical result.

The percentage of each mode accounting for the total axial displacement was also calculated in the simulation and is plotted in Figure 10, where both L(0, 2) and F(1, 3) modes take the main proportion of the total amplitude with the total percentage up to 50%. The first three modes increase slightly with the crack length, while the F(3, 3), F(4, 3) and F(5, 3) modes show the opposite trend. The proportions of the flexural wave modes are similar to those in the analytical results, in which F(2, 3) and F(3, 3) are

about 5% and 10% lower than the longitudinal mode. Nevertheless, the first three modes still dominate the induced nonlinearity and none of them can be ignored when evaluating the severity of a closed crack.

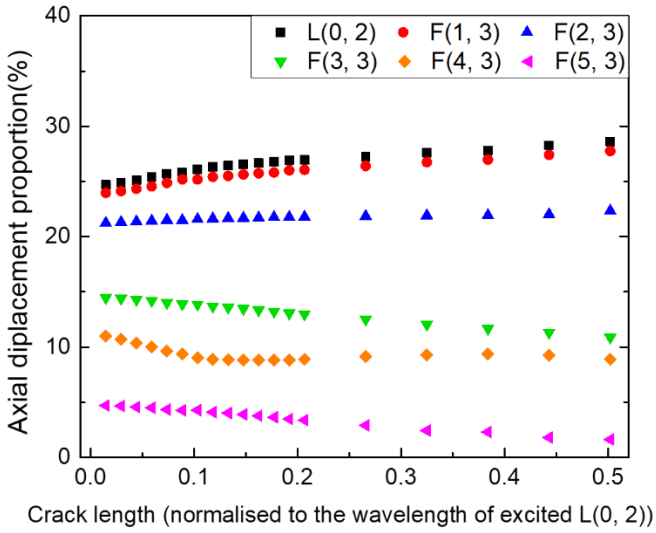


Figure 10 Axial displacement proportion of different wave modes at double frequency with various crack lengths from simulation results.

## 5. Discussion

### *5.1 Comparison of analytical and numerical results*

To further analyse the difference between the analytical and simulation results, the normalised axial displacement changes of each wave mode with different crack lengths from both methods are compared in Figure 11.

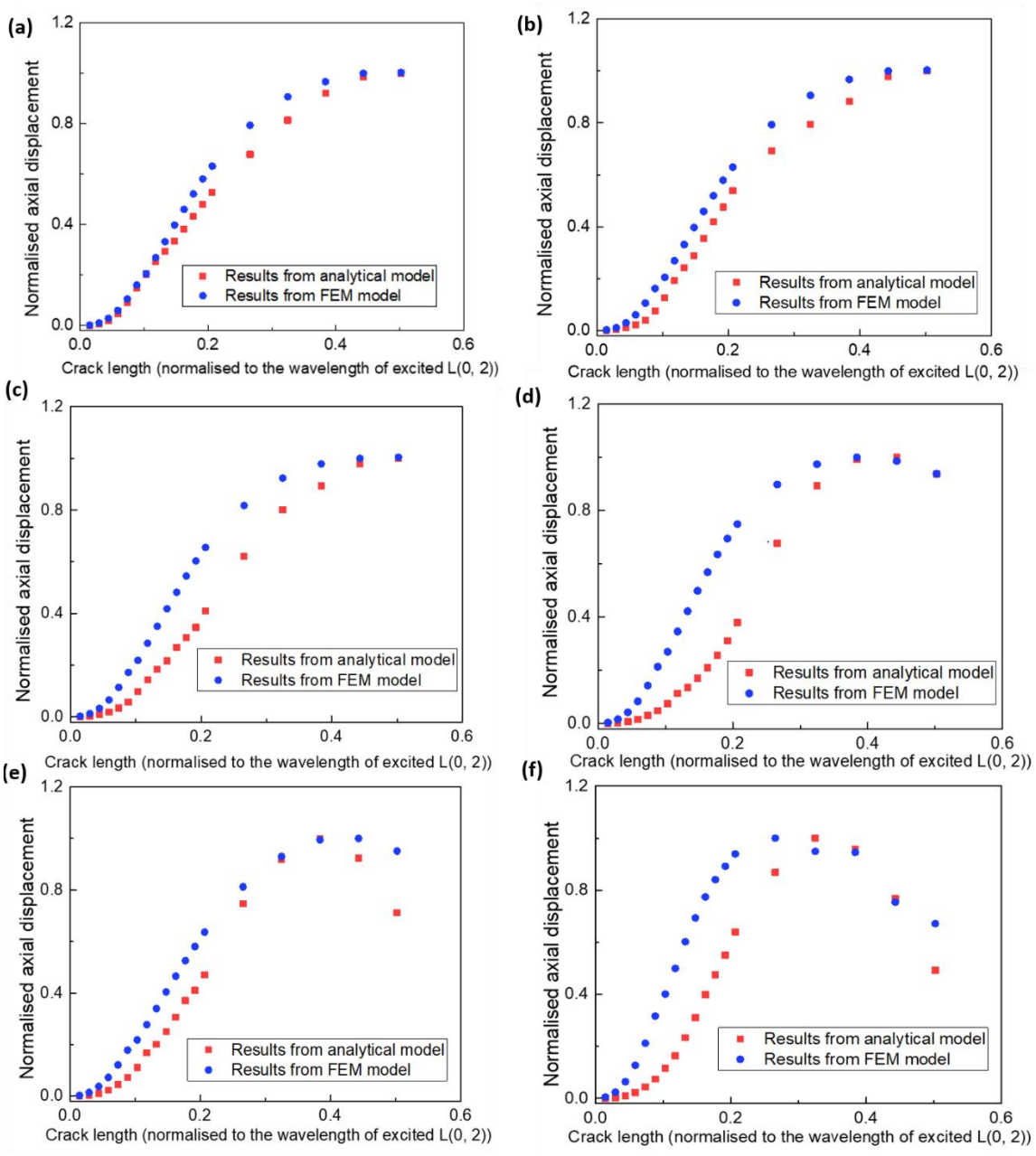


Figure 11 Comparison of normalised axial displacement amplitudes from numerical and theoretical analyses for (a) L(0, 2) mode; (b) F(1, 3) mode; (c) F(2, 3) mode; (d) F(3, 3) mode; (e) F(4, 3) mode and (f) F(5, 3) mode.

As seen in the figures, the first three modes have similar trends for simulation and theoretical results. However, for the higher order flexural waves (n>2), the differences are more obvious than in the first three modes. The theoretical values are lower than

their simulation counterparts. Apart from the unavoidable errors during the separation of each mode, another reason is mainly that the stress on the crack was assumed to be uniformly distributed for the theoretical analysis whereas the stress could not be ideally uniform due to the beam spreading of the wave excited by a point load and the blind zone between each element in the excitation for the simulation model [59].

In order to investigate the influence of beam spreading and the blind zone on the stress distribution of the crack, the distance between the excitation ring and the crack was adjusted. To achieve this, another transducer ring was added to the same model at the distance of 100 mm from the crack, that is, 200 mm closer than the original position. The displacement of the second harmonic wave L(0, 2) in this case compared with the original distance is shown in Figure 12. As can been seen in the figure, when the actuator ring approaches the crack, the differences between the analytical and simulation results increase due to the less uniform distribution of stress on the crack which is induced by the closer excitation, revealing that the location of the actuator ring influences the stress distribution on the crack and the CAN generated by the crack.

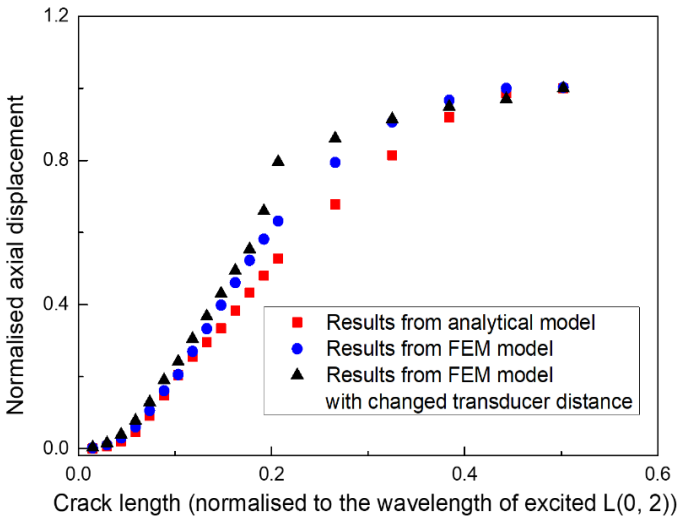

Figure 12 Influence of distance between transducer ring and the crack location. The transducer location is same for analytical and FEM model. After changing the transducer distance to the crack in FEM model, the axial displacement also changes.

Another possible reason for the difference between the analytical and FE models is that the simulation results for higher order flexural wave modes may be unstable due to the heavily dispersive properties of those modes, so that, when compared with the analytical model, the higher order flexural modes show relatively greater error than the longitudinal and lower order flexural modes ($n \leq 2$). However, from the proportion evaluation of each mode that contributes to the nonlinearity in both methods, L(0, 2), F(1, 3) and F(2, 3) modes play the major role and show monotonous increases in contrast to the higher order flexural modes.

Nevertheless, the amplitude trends of different modes generated at double frequency from theoretical model are observed to be consistent with the simulation model, especially for longitudinal and lower order flexural modes ($n \leq 2$). The FE simulation model confirms the phenomena observed from the analytical model, which includes the generation of multiple modes at double frequency and the changing trends of the amplitudes of these modes with crack length. The differences between analytical and simulation results are acceptable because the analytical model is a simplified model with the assumption of uniform stress distribution on the crack without considering the possible bending caused by the flexural modes, which may complicate the closing and opening behaviour of the crack. Both the simulation and analytical model results reveal that, in the pipe structure with a breathing crack, multiple modes are generated at double

frequency with single longitudinal mode excitation, and it is noticed that the generated amplitudes of lower order flexural modes are comparable with that of the zero order longitudinal mode at double frequency.

It is worthy noted that although in practice, the single microcrack generally initiates at the location of stress concentration, such as the edge of notches or holes, only the breathing microcrack was considered in the analytical and numerical models of this work. Aiming to investigate the theoretical basis for the CAN caused by microcrack in pipe structures, the notch or hole was not simulated in the model since they would not influence the nonlinearity measurement in the received signal.

### *5.2 Nonlinear index for pipe structures*

In the literature, the severity of nonlinearity in a system was measured with a nonlinear parameter, such as the nonlinear parameter β in isotropic plates [60, 61] and composites [62], which is the ratio of the peak value of the amplitude of the second harmonic wave to the square of the peak value of the amplitude of the fundamental wave. In a pipe structure with rings of multiple transducers and sensors, the possible number of second harmonic modes can be predicted through the dispersion curve, and the received second harmonic modes would be separated by the use of appropriate signal acquisition methods. However, when one actuator and one sensor in a line are used for damage detection in pipe structures, as is usually adopted in experiments with PZT transducers, the received signals are more complex where more than one wave packet may present because the group velocities of each mode are too similar to separate. As a result, it is

difficult to calculate the nonlinear parameter based on a single peak value of the amplitude. A new and more suitable parameter is required to measure the nonlinearity.

In this circumstance, a parameter considering all generated wave packets is proposed, which is the integral of the amplitude profile of the second harmonic wave of interest within a time period (denoted as $S_{2f}$) divided by the integral of the amplitude profile of the fundamental wave (denoted as $S_f$). A simulation example is proposed here, which has the same configuration as the model in this study, but where only one sensor was used. In this case, the seam crack length was 10 mm and the pure longitudinal wave L(0, 2) generated multiple wave modes at double frequency, including L(0, 2) and flexural modes F(n, 3). One of the received signals was processed through a short-time Fourier transform (STFT) and signals at fundamental and double frequency were extracted and plotted in the time domain using a Hilbert transform, as shown in Figure 13.

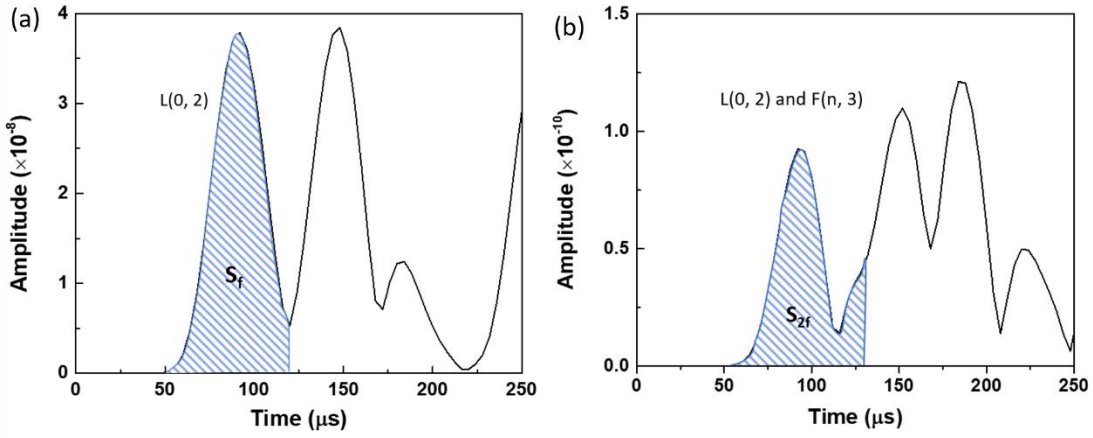


Figure 13 Signals from simulation model for 10 mm seam crack case after STFT at (a) fundamental frequency and (b) double frequency. The shadow areas include the L(0, 2) wave

packet at fundamental frequency ($S_f$), and L(0, 2) and F(n, 3) wave packets at double frequency ($S_{2f}$).

Therefore, the new nonlinear index can be calculated as

$$Nonlinear\ \ index = \frac{S_{2f}}{S_f} \tag{9}$$

Following Equation 9, the nonlinear index can be calculated, but it should be noted that this index should be used with a certain time window of interest. In this case, the end point of the time window for the signal at double frequency was selected at the time when L(0, 1) wave mode arrived, calculated from the theoretical group velocity in the dispersion curve, which is slower than all possible higher order flexural modes induced by the crack at double frequency, so as to include all these induced modes at double frequency. Instead of using the amplitude of one wave mode as the nonlinear parameter β, this index considers all the possible second harmonic wave modes which are commonly observed in a pipe structure with a circumferential closed crack, so as to avoid underestimating the contribution of flexural modes to the nonlinearity. This nonlinear index was deployed in a previous study [30] where the experiment results verified the efficiency of the proposed nonlinear index for the severity evaluation of initial fatigue crack in pipe structures.

## 6. Conclusions

To provide an in-depth understanding of the mechanism of a breathing microcrack on the nonlinear properties of the guided waves in pipe structures, a simplified analytical model was developed for longitudinal wave interaction with a circumferential breathing

crack in a pipe. The idea was based on an analytical model in a plate with CAN and wave scattering in a pipe by a circumferential crack using linear methods. The S-parameter was used to calculate the amplitude of each second harmonic mode induced by the breathing crack, followed by a simulation study with the same configuration model as in the analytical analysis. The results from the two methods were compared and the differences were discussed.

The analytical model was useful for describing the interaction between longitudinal wave and the breathing crack. It also showed that the second harmonic waves contained different modes in a pipe structure and the flexural wave modes occupied a high proportion of the total energy induced by CAN. Based on this analysis, a new nonlinear index more suitable for the measurement of CAN in pipe structures was proposed for use when multiple wave modes cannot be appropriately separated. This nonlinear index, deployed in a previous experimental test, clearly explains the indispensable effect of the flexural modes on the CAN. Therefore, the flexural modes must be considered in the nonlinear index for micro damage evaluation. This study provides insight and strong theoretical basis of CAN characteristics in pipe structures which can assist interpretation of received signal for damage identification in practice. This facilitates continuous and quantitative monitoring of fatigue damage, particularly at its onset stage, which will benefit residual life evaluation and prognosis of structures.

## Acknowledgement

This work is supported by the Early Career Scheme of the Research Grants Council of Hong Kong (grant no. 25211319).

## References

[1] Chillara VK,Lissenden CJ, Interaction of guided wave modes in isotropic weakly nonlinear elastic plates: Higher harmonic generation. J Appl Phys 2012; 111: 124909, https://doi.org/10.1063/1.4729554.
[2] Soleimanpour R,Ng CT, Locating delaminations in laminated composite beams using nonlinear guided waves. Eng Struct 2017; 131: 207-19, https://doi.org/10.1016/j.engstruct.2016.11.010.
[3] Gao GJ, Liu C, Hu N, Deng MX, Chen H,Xiang YX, Response of second-harmonic generation of Lamb wave propagation to microdamage thickness in a solid plate. Wave Motion 2020; 96: 102557, https://doi.org/10.1016/j.wavemoti.2020.102557.
[4] Kim J, Zhu B,Cho YH, An experimental study on second harmonic generation of guided wave in fatigued spring rod. J Mech Sci Technol 2019; 33: 4105-9, https://doi.org/10.1007/s12206-019-0805-0.
[5] Yang Y, Ng C-T,Kotousov A, Second harmonic generation of guided wave at crack-induced debonding in FRP-strengthened metallic plates. Int J Struct Stab Dyn 2019; 19: 1940006, https://doi.org/10.1142/S0219455419400066.
[6] Yang Y, Ng CT,Kotousov A, Bolted joint integrity monitoring with second harmonic generated by guided waves. Struct Health Monit 2019; 18: 193-204, https://doi.org/10.1177/1475921718814399.
[7] Hasanian M,Lissenden CJ, Directional nonlinear guided wave mixing: Case study of counter-propagating shear horizontal waves, in AIP Conference Proceedings, Vol.1949, 2018.
[8] Lissenden CJ, Liu Y, Chillara VK, Choi G,Cho H, Nonlinear guided wave mixing for localized material state characterization. Physcs Proc 2015; 70: 668-71, https://doi.org/10.1016/j.phpro.2015.08.074.
[9] Cho H, Hasanian M, Shan SB,Lissenden CJ, Nonlinear guided wave technique for localized damage detection in plates with surface-bonded sensors to receive Lamb waves generated by shear-horizontal wave mixing. Ndt&E Int 2019; 102: 35-46, https://doi.org/10.1016/j.ndteint.2018.10.011.
[10] Ding XY, Zhao YX, Deng MX, Shui GS,Hu N, One-way Lamb mixing method in thin plates with randomly distributed micro-cracks. Int J Mech Sci 2020; 171: 105371, https://doi.org/10.1016/j.ijmecsci.2019.105371.
[11] Li W, Xu Y, Hu N,Deng M, Impact damage detection in composites using a guided wave mixing technique. Meas Sci Technol 2019; 31: 014001, https://doi.org/10.1088/1361-6501/ab382e.
[12] Shan S, Hasanian M, Cho H, Lissenden CJ,Cheng L, New nonlinear ultrasonic method for material characterization: Codirectional shear horizontal guided wave

mixing in plate. Ultrasonics 2019; 96: 64-74, https://doi.org/10.1016/j.ultras.2019.04.001.
[13] Shen YF, Wang JZ,Xu W, Nonlinear features of guided wave scattering from rivet hole nucleated fatigue cracks considering the rough contact surface condition. Smart Mater Struct 2018; 27: 105044, https://doi.org/10.1088/1361-665X/aadd2d.
[14] Zhang MY, Xiao L, Qu WZ,Lu Y, Damage detection of fatigue cracks under nonlinear boundary condition using subharmonic resonance. Ultrasonics 2017; 77: 152-9, https://doi.org/10.1016/j.ultras.2017.02.001.
[15] Maruyama T, Saitoh T,Hirose S, Numerical study on sub-harmonic generation due to interior and surface breaking cracks with contact boundary conditions using time-domain boundary element method. Int J Solids Struct 2017; 126-127: 74-89, https://doi.org/10.1016/j.ijsolstr.2017.07.029.
[16] Broda D, Staszewski WJ, Martowicz A, Uhl T,Silberschmidt VV, Modelling of nonlinear crack-wave interactions for damage detection based on ultrasound-A review. J Sound Vib 2014; 333: 1097-118, https://doi.org/10.1016/j.jsv.2013.09.033.
[17] Muller MF, Kim JY, Qu J,Jacobs LJ, Characteristics of second harmonic generation of Lamb waves in nonlinear elastic plates. J Acoust Soc Am 2010; 127: 2141-52, https://doi.org/10.1121/1.3294714.
[18] Matlack KH, Kim JY, Jacobs LJ,Qu JM, Experimental characterization of efficient second harmonic generation of Lamb wave modes in a nonlinear elastic isotropic plate. J Appl Phys 2011; 109: 014905, https://doi.org/10.1063/1.3527959.
[19] Chakrapani SK,Barnard DJ, Determination of acoustic nonlinearity parameter (β) using nonlinear resonance ultrasound spectroscopy: Theory and experiment. J Acoust Soc Am 2017; 141: 919-28, https://doi.org/10.1121/1.4976057.
[20] Zhu W, Deng M, Xiang Y, Xuan FZ, Liu C,Wang YN, Modeling of ultrasonic nonlinearities for dislocation evolution in plastically deformed materials: Simulation and experimental validation. Ultrasonics 2016; 68: 134-41, https://doi.org/10.1016/j.ultras.2016.02.016.
[21] Richardson JM, Harmonic generation at an unbonded interface—I. Planar interface between semi-infinite elastic media. Int J Eng Sci 1979; 17: 73-85, https://doi.org/10.1016/0020-7225(79)90008-9.
[22] Rudenko OV,Vu CA, Nonlinear acoustic properties of a rough surface contact and acoustodiagnostics of a roughness height distribution. Acoust Phys 1994; 40: 593-6, https://doi.org/10.1016/j.phpro.2015.08.286.
[23] Solodov IY, Krohn N,Busse G, CAN: an example of nonclassical acoustic nonlinearity in solids. Ultrasonics 2002; 40: 621-5, https://doi.org/10.1016/S0041-624x(02)00186-5.
[24] Zhang Z, Nagy PB,Hassan W, Analytical and numerical modeling of non-collinear shear wave mixing at an imperfect interface. Ultrasonics 2016; 65: 165-76, https://doi.org/10.1016/j.ultras.2015.09.021.
[25] Aleshin V, Delrue S, Trifonov A, Matar OB,Van Den Abeele K, Two dimensional modeling of elastic wave propagation in solids containing cracks with rough surfaces and friction - Part I: Theoretical background. Ultrasonics 2018; 82: 11-8, https://doi.org/10.1016/j.ultras.2017.07.002.

[26] Wang K, Li Y, Su Z, Guan R, Lu Y,Yuan S, Nonlinear aspects of “breathing” crack-disturbed plate waves: 3-D analytical modeling with experimental validation. Int J Mech Sci 2019; 159: 140-50, https://doi.org/10.1016/j.ijmecsci.2019.05.036.
[27] Liu Y, Lissenden CJ,Rose JL, Higher order interaction of elastic waves in weakly nonlinear hollow circular cylinders. I. Analytical foundation. J Appl Phys 2014; 115: 214901, https://doi.org/10.1063/1.4879459.
[28] Liu Y, Khajeh E, Lissenden CJ,Rose JL, Higher order interaction of elastic waves in weakly nonlinear hollow circular cylinders. II. Physical interpretation and numerical results. J Appl Phys 2014; 115: 214902, https://doi.org/10.1063/1.4879460.
[29] Liu Y, Khajeh E, Lissenden CJ,Rose JL, Interaction of torsional and longitudinal guided waves in weakly nonlinear circular cylinders. J Acoust Soc Am 2013; 133: 2541-53, https://doi.org/10.1121/1.4795806.
[30] Guan R, Lu Y, Wang K,Su Z, Quantitative fatigue crack evaluation in pipeline structures using nonlinear cylindrical waves. Smart Mater Struct 2018; 28: 025015, https://doi.org/10.1088/1361-665X/aaf242.
[31] Guan RQ, Lu Y, Wang K,Su ZQ, Fatigue crack detection in pipes with multiple mode nonlinear guided waves. Struct Health Monit 2019; 18: 180-92, https://doi.org/10.1177/1475921718791134.
[32] Gao K, Rougier E, Guyer RA, Lei Z,Johnson PA, Simulation of crack induced nonlinear elasticity using the combined finite-discrete element method. Ultrasonics 2019; 98: 51-61, https://doi.org/10.1016/j.ultras.2019.06.003.
[33] Shen YF,Cesnik CES, Nonlinear scattering and mode conversion of Lamb waves at breathing cracks: An efficient numerical approach. Ultrasonics 2019; 94: 202-17, https://doi.org/10.1016/j.ultras.2018.09.011.
[34] Shen YF,Cesnik CES, Modeling of nonlinear interactions between guided waves and fatigue cracks using local interaction simulation approach. Ultrasonics 2017; 74: 106-23, https://doi.org/10.1016/j.ultras.2016.10.001.
[35] Shen Y,Cesnik CE, Local interaction simulation approach for efficient modeling of linear and nonlinear ultrasonic guided wave active sensing of complex structures. ASME J Nondestructive Evaluation 2018; 1: https://doi.org/10.1115/1.4037545.
[36] Kimoto K,Ichikawa Y, A finite difference method for elastic wave scattering by a planar crack with contacting faces. Wave Motion 2015; 52: 120-37, https://doi.org/10.1016/j.wavemoti.2014.09.007.
[37] Sarens B, Verstraeten B, Glorieux C, Kalogiannakis G,Van Hemelrijck D, Investigation of contact acoustic nonlinearity in delaminations by shearographic imaging, laser doppler vibrometric scanning and finite difference modeling. IEEE Trans Ultrason Ferroelectr Freq Control 2010; 57: 1383-95, https://doi.org/10.1109/TUFFC.2010.1557.
[38] He S,Ng CT, Modelling and analysis of nonlinear guided waves interaction at a breathing crack using time-domain spectral finite element method. Smart Mater Struct 2017; 26: 085002, https://doi.org/10.1088/1361-665X/aa75f3.
[39] Yuan M, Lee T, Kang T, Zhang J, Song S-J,Kim H-J, Absolute measurement of ultrasonic non-linearity parameter at contact interface. Nondestruct Test Eva 2015; 30: 356-72, https://doi.org/10.1080/10589759.2015.1041523.

[40] Hong M, Su Z, Wang Q, Cheng L,Qing X, Modeling nonlinearities of ultrasonic waves for fatigue damage characterization: theory, simulation, and experimental validation. Ultrasonics 2014; 54: 770-8, https://doi.org/10.1016/j.ultras.2013.09.023.
[41] Singh AK, Chen BY, Tan VB, Tay TE,Lee HP, Finite element modeling of nonlinear acoustics/ultrasonics for the detection of closed delaminations in composites. Ultrasonics 2017; 74: 89-98, https://doi.org/10.1016/j.ultras.2016.09.019.
[42] Zhang Z, Xiao Y, Xie YH,Su ZQ, Effects of contact between rough surfaces on the dynamic responses of bolted composite joints: Multiscale modeling and numerical simulation. Compos Struct 2019; 211: 13-23, https://doi.org/10.1016/j.compstruct.2018.12.019.
[43] Gschossmann S, Oberascher T,Schagerl M, Quantification of subsurface cracks in a thin aluminium beam by the use of nonlinear guided wave theory–a numerical and model-based approach, in Proceedings of the 9th EWSHM, Vol.10, 2018.
[44] Broda D, Pieczonka L, Hiwarkar V, Staszewski WJ,Silberschmidt VV, Generation of higher harmonics in longitudinal vibration of beams with breathing cracks. J Sound Vib 2016; 381: 206-19, https://doi.org/10.1016/j.jsv.2016.06.025.
[45] Wang K, Fan Z,Su ZQ, Orienting fatigue cracks using contact acoustic nonlinearity in scattered plate waves. Smart Mater Struct 2018; 27: 09LT1, https://doi.org/10.1088/1361-665X/aad52f.
[46] Meziane A, Norris A,Shuvalov A, Nonlinear shear wave interaction at a frictional interface: Energy dissipation and generation of harmonics. J Acoust Soc Am 2011; 130: 1820-8, https://doi.org/10.1121/1.3628663.
[47] Blanloeuil P, Meziane A, Norris AN,Bacon C, Analytical extension of Finite Element solution for computing the nonlinear far field of ultrasonic waves scattered by a closed crack. Wave Motion 2016; 66: 132-46, https://doi.org/10.1016/j.wavemoti.2016.04.016.
[48] Blanloeuil P, Rose LRF, Veidt M,Wang CH, Analytical and numerical modelling of wave scattering by a linear and nonlinear contact interface. J Sound Vib 2019; 456: 431-53, https://doi.org/10.1016/j.jsv.2019.05.048.
[49] Delrue S, Aleshin V, Truyaert K, Matar OB,Van Den Abeele K, Two dimensional modeling of elastic wave propagation in solids containing cracks with rough surfaces and friction - Part II: Numerical implementation. Ultrasonics 2018; 82: 19-30, https://doi.org/10.1016/j.ultras.2017.07.003.
[50] Yuan M, Zhang J, Song S-J,Kim H-J, Numerical simulation of Rayleigh wave interaction with surface closed cracks under external pressure. Wave Motion 2015; 57: 143-53, https://doi.org/10.1016/j.wavemoti.2015.03.009.
[51] Ditri JJ, Utilization of guided elastic-waves for the characterization of circumferential cracks in hollow cylinders. J Acoust Soc Am 1994; 96: 3769-75, https://doi.org/10.1121/1.410565.
[52] Gazis DC, Three-dimensional investigation of the propagation of waves in hollow circular cylinders. I. Analytical foundation. J Acoust Soc Am 1959; 31: 568-73, https://doi.org/10.1121/1.1907753.

[53] Wang K, Liu M, Su Z, Yuan S,Fan Z, Analytical insight into “breathing” crack-induced acoustic nonlinearity with an application to quantitative evaluation of contact cracks. 2018; 88: 157-67, https://doi.org/https://doi.org/10.1016/j.ultras.2018.03.008.
[54] Yoo SH,Pan J, Approximate crack opening displacement solutions for long circumferential cracks in pipes subjected to bending and tension. J Press Vess-T Asme 1992; 114: 178-80, https://doi.org/10.1115/1.2929026.
[55] Sanders JL, Circumferential through-cracks in cylindrical-shells under tension. J Appl Mech-T Asme 1982; 49: 103-7, https://doi.org/10.1115/1.3161948.
[56] Rose JL, Ultrasonic guided waves in solid media, Cambridge University Press, New York, 2014.
[57] Alleyne DN, Lowe MJS,Cawley P, The reflection of guided waves from circumferential notches in pipes. J Appl Mech-T Asme 1998; 65: 635-41, https://doi.org/10.1115/1.2789105.
[58] Lowe MJS, Alleyne DN,Cawley P, The mode conversion of a guided wave by a part-circumferential notch in a pipe. J Appl Mech-T Asme 1998; 65: 649-56, https://doi.org/10.1115/1.2789107.
[59] Kino GS, Acoustic waves: devices, imaging, and analog signal processing, Prentice-hall Englewood Cliffs, NJ, 1071987.
[60] Bermes C, Kim JY, Qu JM,Jacobs LJ, Experimental characterization of material nonlinearity using Lamb waves. Appl Phys Lett 2007; 90: 021901, https://doi.org/10.1063/1.2431467.
[61] Murnaghan FD, Finite deformations of an elastic solid. Am J Math 1937; 59: 235-60, https://doi.org/10.2307/2371405.
[62] Li W, Cho Y,Achenbach JD, Detection of thermal fatigue in composites by second harmonic Lamb waves. Smart Mater Struct 2012; 21: 085019, https://doi.org/10.1088/0964-1726/21/8/085019.